ELSEVIER

Chemical Engineering Journal 94 (2003) 79–92

Chemical Engineering Journal

www.elsevier.com/locate/cej

A study on dissolution kinetics of carbon in liquid iron bath

D. Bandyopadhyay [a,*], S.D. Singh [a], D. Sanyal [b], K.K. Singh [a], K.N. Singh [c]

[a] *Ferrous Process Division, National Metallurgical Laboratory, Jamshedpur 831007, India*
[b] *Regional Liaison Centre, National Metallurgical Laboratory, Kolkata 700001, India*
[c] *Department of Metallurgical Engineering, Regional Engineering College, Rourkela, India*

Received 16 April 2001; accepted 11 February 2002

Abstract

Dissolution of carbon in liquid iron melt is one of the very important reactions in chemical and metal processing industries, as it decides, in many cases, the productivity of a process or quality of the product. As a result, the current investigation was undertaken to study the effect of different physical and chemical characteristics of five types of carbon sources on dissolution kinetics. Bath chemistry being a very important factor in determining the process, two types of iron bearing materials, namely, electrolytic iron and sponge iron were employed for the study. It has been found that though the ash in carbon exhibits significant effect on carbon dissolution, the influence of the volatile matter was not found to be noteworthy. It has also been observed that petroleum coke undergoes maximum dissolution possibly due to its porous structure as well as less amount of inherent impurity. Silicon is found to be a strong promoter of the kinetics whereas the depressing effect of sulphur is not found to be that pronounced. Preliminary results of a mathematical model shows that the dissolution in Tamman furnace takes place under constant heat flux condition.

Keywords: Dissolution; Kinetics; Smelting–reduction; Carbon

1. Introduction

The dissolution of carbon in molten iron bath is one of the important reactions in the chemical and metal processing industries and has assumed special significance in the last two decades in the light of new technological developments around the world. To cite a few practical examples: coal gasification in iron bath involves dissolution of carbon in the liquid iron bath where it reacts with the dissolved oxygen to form carbon monoxide. When oxygen is blown in iron–carbon melt, an exothermic reaction takes place and thus, there is a possibility of using increasing amount of scrap in oxygen steel making. The latest trend in non-conventional iron making route is smelting–reduction process where iron oxide in liquid iron bath gets reduced with the help of dissolved carbon. The success of this process depends greatly depends on the rate of carbon dissolution in liquid iron as it decides the rate of carbon supply for reduction of iron oxide and thus the productivity. In shaft furnaces like blast furnaces and cupola, carbon dissolution from coke takes place where liquid iron droplets are in direct contact with carbon. For many foundry practices, carbon pick up by hot metal is a limiting factor because the machinability depends on the amount of carbon and it should be high for good machining characteristics. On the other hand, carbon dissolution by hot metal should be avoided in certain situations. For example, in the well zone of blast furnace extensive carbon pick up from carbon blocks will lead to break down.

Many investigators [1–11] have studied the effect of inherent physical properties of different forms of carbon, bath composition, state-of-bath, etc. on dissolution kinetics. But it has been found that anomalies still exist on many major issues such as the effect of sulphur, carbon structure, role of volatile matter, etc. on the carbon dissolution. In the present investigation, an attempt has been made to reinvestigate some of the controversies employing carbon sample widely varying in chemical composition as well as in structure. Further, a comprehensive mathematical model has been developed involving heat and mass transfer phenomena. Salient aspects of the model have been presented briefly in this paper to perform preliminary analyses for mass transfer coefficient and thermal state-of-bath.

2. Experimental

2.1. Raw materials

In the present series of experiments, five different types of carbonaceous materials were used. The carbon types were

* Corresponding author. Tel.: +91-657-27-0096; fax: +91-657-27-0527.
E-mail address: db@csnml.ren.nic.in (D. Bandyopadhyay).

1385-8947/02/$ – see front matter
doi:10.1016/S1385-8947(02)00030-X

Table 1
Proximate analysis of carbonaceous materials

Serial number	Types of carbon	Proximate analysis (%)					
		FC	VM	Ash	Moisture	S	P
1	Nut coke	73.68	1.2	24.8	0.32	0.11	0.26
2	Charcoal	59.96	32.29	3.75	4.00	0.41	Trace
3	Pet coke	97.20	2.50	0.24	0.06	0.66	Trace
4	Coal	50.7	33.15	13.47	2.68	0.43	–
5	Graphite	99.03	0.43	0.46	0.08	Trace	–

so chosen that the ash and the volatile matter varied over a very wide range. The proximate analyses of the carbons used in the dissolution study are summarised in Table 1. Commercially available graphite rods of 19.5 mm diameter were directly used in the study. Other forms of carbon namely, pet coke, nut coke, charcoal and coal were hand-ground to approximately cylindrical shape of 20 mm diameter and 50 mm length.

Two types of iron bearing materials namely electrolytic iron and sponge iron were employed for generation of dissolution media. Composition of both the iron bearing materials are presented in Table 2.

Laboratory grade FeSi and FeS were used as additives to study the effect of S and Si on the dissolution process. Both the additives were supplied in form of lump and were powdered before addition.

2.2. Experimental procedures

The carbon dissolution experiments were conducted in Tamman furnace, schematically shown in Fig. 1. This being resistive heating type, provides a relatively quiet bath. An amount of 750 g of electrolytic iron powder or 500 g of sponge iron contained in a high alumina crucible, capable of withstanding 1800 °C was put in the constant temperature zone of the furnace at room temperature. The alumina crucible was 60 mm in internal diameter and 95 mm in height. Two B-type thermocouples, one for controlling the furnace and the other for temperature measurement were used during experiments. The control thermocouple was placed between the heating element and the alumina crucible and was connected to a Eurotherm made PID temperature controller. It was observed that in the experimental temperature range, the furnace could be controlled within ±2 °C. Experiments were conducted at three temperatures namely, 1550, 1600 and 1650 °C. The furnace was heated to the desired temperature at a rate of approximately 15 °C/min under continuous argon purging. Inert gas flow was maintained to minimise the oxidation of iron bearing material, carbon sample as well as of the carbon heating element. After the melt down of iron, time was allowed for thermal stabilisation of the bath before any carbon addition. Liquid samples ware taken by suction for initial bath carbon determination. Carbon samples were then immersed in the liquid bath. All the carbon samples were dipped in the bath for 12 min. Samples were preheated before dipping in the melt by holding them over the bath for few minutes. This was done to prevent excessive bath boiling due to immersion of cold sample. Graphite sample in the form of electrode could be directly dipped in

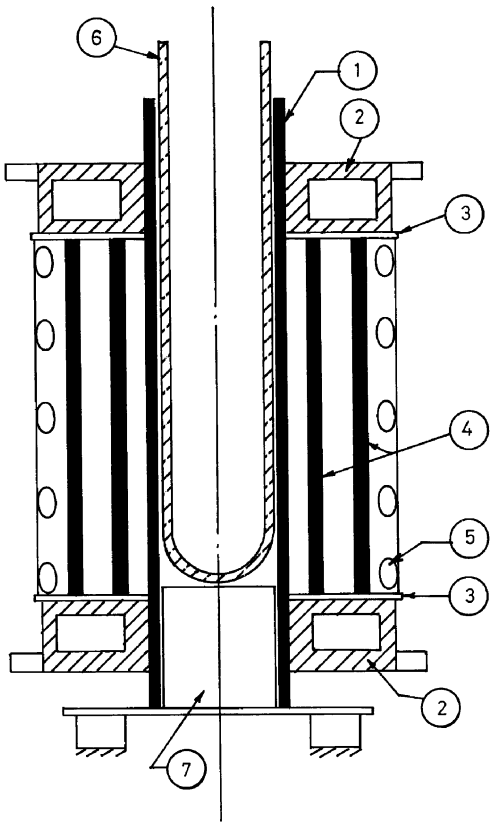

Fig. 1. Schematic diagram of a Tamman furnace.

Table 2
Chemical analysis of iron bearing materials

Serial number	Type of iron material	Constituents (%)						
		C	S	P	SiO_2	CaO	MgO	Al_2O_3
1	Sponge iron	0.20	0.02	0.03	2.35	0.36	0.80	0.66
2	Electrolytic iron	0.015	0.045	Trace	Trace	NF	Trace	–

NF: not found.

the liquid bath whereas all other types of carbon samples of approximately cylindrical shape were force-fitted in an alumina tube of appropriate size. Liquid iron samples were drawn from the bath at regular time interval. Bath carbon as a function of time was determined by chemical analysis of the iron samples using LECO carbon sulphur analyser.

3. Results of experiments

As mentioned earlier, five types of carbons were used in the present investigation to study the effect of different physical properties of carbon on dissolution kinetics. Fig. 2 presents the bath carbon as a function of time for all the five types of carbon at 1600 °C.

It may be noted from Fig. 2 that pet coke exhibits the highest dissolution rate whereas the same for nut coke is minimum. Dissolution rates of graphite, charcoal and coal fall in between in decreasing order. It has been reported in literature [1–3,7,8] that carbon structure and extent of porosity significantly alter the dissolution kinetics. Further, it is to be noted that the dissolution process also depends on number of other characteristics of carbon such as ash content, its constituents and the fusion point, extent of volatile matter, fixed carbon, etc. All these parameters have interactive influence on the kinetics. However, in the following discussion, it has been attempted to address these parameters individually.

It has been reported [2,3] that at high temperature, ash in carbon undergoes fusion and forms a viscous layer around the solid–liquid interface. This acts as a barrier between the carbon surface and the iron melt. A similar observation has been reported by Mourao et al. [11]. Hence, carbon with less amount of ash is expected to dissolve faster. This point is well illustrated by the present set of experimental data. It is apparent from Table 1 that ash content of pet coke is much lower in comparison with other forms of carbon such as coal and nut coke. As a consequence, pet coke dissolves at a much faster rate than samples like nut coke or coal under identical experimental conditions. Further, the extent of hindrance offered by the viscous ash layer to dissolution also depends on its fusion point. Ash in carbon with low fusion point gets removed relatively easily in the form of slag by the bath movement and permits continuos renewal of the carbon surface in contact with the iron melt. Hence, any reagent which lowers the fusion point of ash is expected to promote dissolution. However, it should be borne in mind that ash content in the carbon is only one of the factors that affects the dissolution kinetics.

Volatile matter is also reported [6] to inhibit the dissolution process due to formation of a gas film around the carbon. In the present investigation, volatile matter appears to have an insignificant influence on the kinetics. This becomes apparent by comparing the volatile matter content of charcoal, coal and nut coke (Table 1) with their respective dissolution data (Fig. 2). Nut coke contains very low volatile matter compared to charcoal and coal but dissolution rate of the same is the slowest in the lot. This observation suggests that the samples got completely or very significantly devolatilised during the early stage of immersion, leading to negligible influence on dissolution kinetics.

Contradictory observations have been reported in the literature on the effect of carbon porosity on dissolution. Kayama et al. [9] observed that coke with low porosity has a high rate of dissolution. On the contrary, Mourao et al. [11] reported that coke with high porosity exhibit higher dissolution and further suggested that higher porosity offers more surface area for reaction and its effect seems to be more significant in the initial period of dissolution. Depending upon

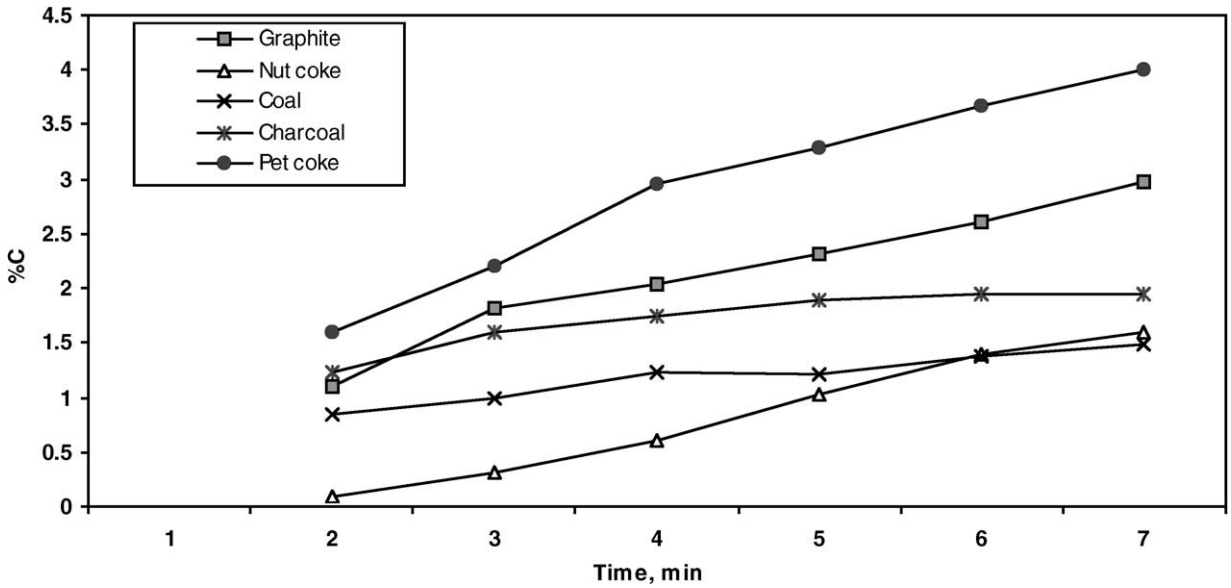

Fig. 2. Carbon concentration of bath against time for different forms of carbon at 1600 °C.

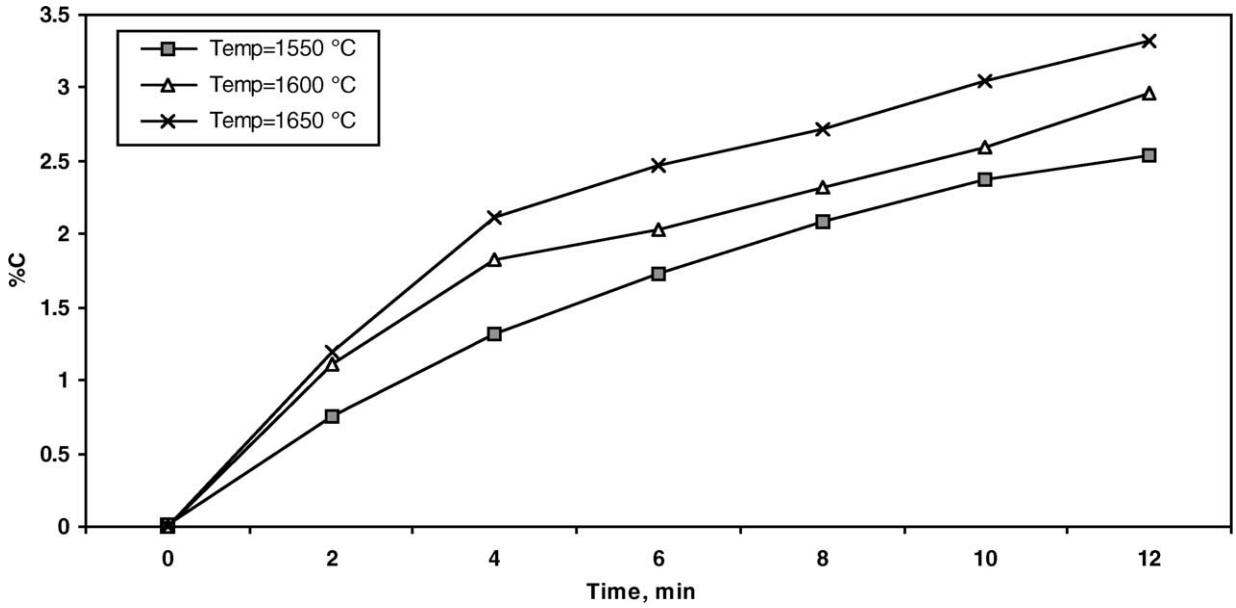

Fig. 3. Effect of temperature on dissolution of graphite in electrolytic iron bath.

the hydrodynamic condition of the bath, liquid metal penetrates the pores and thus, a larger surface area will participate in the reaction. At the later stage, the liquid metal may get trapped in the pores and tend to get saturated by carbon. This will make the inner surface area relatively ineffective. In the present investigation, large porosity in pet coke appears to contribute towards its high dissolution. However, quantitative estimation of the effect of porosity on the kinetics has not been attempted.

Fig. 3 presents the variation of carbon concentration in bath as a function of time, for graphite at three different temperatures. It may be noted from Fig. 3 that as per expectation, the extent of graphite dissolution increases with increase in temperature. Here, it should be mentioned that the temperature range for this investigation was chosen by keeping the industrial operating conditions in mind and is rather narrow. Similar to the observation of Olsson et al. [4], dissolution kinetics appears not to be very significantly altered by the temperature range under consideration.

Fig. 4 shows the effect of sulphur on graphite dissolution in electrolytic iron bath at 1600 °C. It is clear from Fig. 4 that extent of dissolution decreases with addition of 0.05% S in the bath. This observation is in agreement with the reporting of Wright and Badlock [10] for injection of graphite

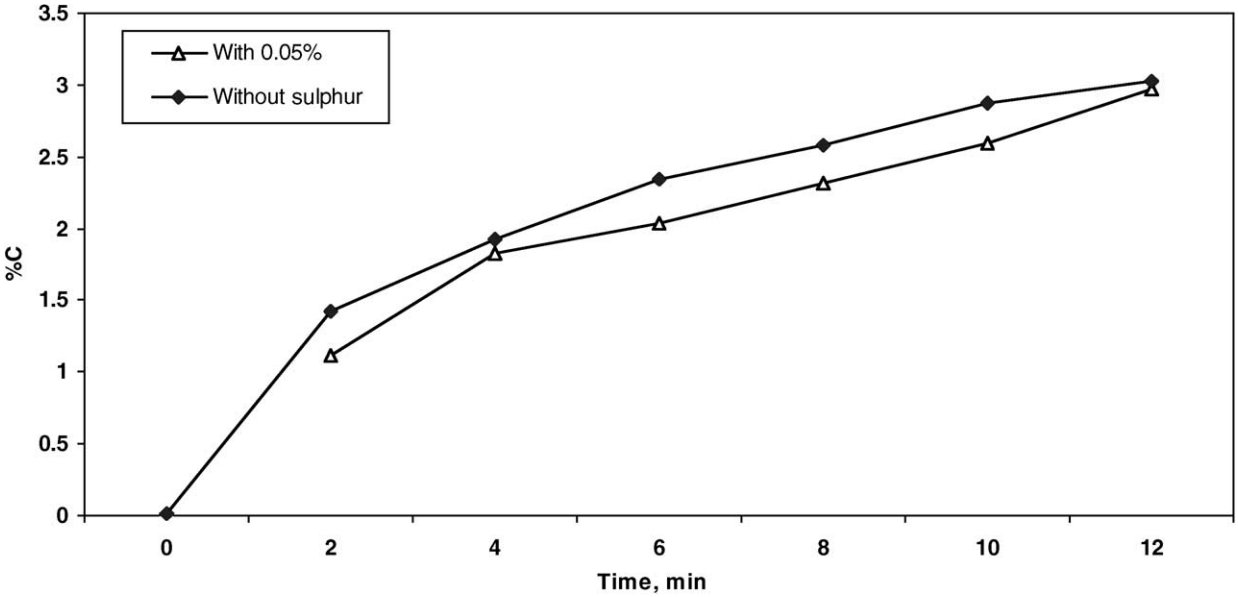

Fig. 4. Effect of sulphur on dissolution of graphite in electrolytic iron bath.

powder and Orsten and Oeters [12] for graphite in sulphur containing iron bath. Similarly, Wright and Baldock [10] have also found that increase of sulphur in bath from 0.1 to 1.0% results in lowering of graphite dissolution at 1450 °C. However, Mourao et al. [11] have reported radically different findings in this regard. The investigators have reported that addition of 0.28% S helped dissolution of graphite in the iron melt. Further addition of sulphur did not affect the dissolution kinetics. Similar observation has also been reported by Kalvelage et al. [13]. Mourao et al. postulated that in the presence of sulphur, a surface active agent, the wettability of graphite surface increases and hence the dissolution rate. However, absence of further supporting observation on enhancing effect of sulphur on graphite dissolution leaves the issue open for further investigation. On the other hand, the same investigators have reported a decrease in coke dissolution rate in the presence of sulphur. Oersten and Oeters [12] have observed that depressing effect of sulphur on non-graphitic carbon is much more pronounced compared to graphite. This phenomenon can possibly be explained in terms of surface conditions of the samples. Graphite being structurally more perfect, offers less active sites for sulphur adsorption. Other forms of carbon, low in degree of graphitisation, contains many surface imperfections such as edge defect, claw defect, twining defect, etc. These imperfections act as active surface sites for sulphur adsorption and consequent lowering of dissolution rate.

Fig. 5 presents the effect of silicon on the dissolution kinetics of graphite in electrolytic iron bath at 1600 °C. It may be noted from Fig. 5 that addition of 0.94% Si enhances dissolution. Si is known to increase the fluidity of the iron melt. With increase in the bath fluidity, the convective flow field will be altered and consequently the concentration profile also. Less viscous bath will develop stronger convective motion under similar energy input condition. This will lead to faster transport of carbon from immediate vicinity of the sample and enhanced dissolution. Finding of Hisatsuna et al. [7] that addition of SiO_2 promotes dissolution of carbon supports the present observation. SiO_2 in presence of dissolved carbon gets reduced to metallic silicon and helps to enhance the fluidity of the bath.

A few experiments were conducted to find the effect of stirring on graphite dissolution at 1600 °C. The result of one such attempt is presented in Fig. 6. In this experiment, the sample was rotated in electrolytic iron bath at 35 rpm. Higher rotation could not be attempted due to size restriction of the container. As expected, the extent of dissolution increased at stirred condition compared to static bath. It is very apparent that graphite exhibits faster dissolution in circulatory bath compared to the static bath.

In an effort to simulate the smelting–reduction bath condition, a few trials were carried out with sponge iron as iron bearing material and two types of carbons namely graphite and nut coke were used in this part of the study. Fig. 7 presents the bath analysis for both the samples. Similar to what has been noticed previously for these samples, extent of nut coke dissolution is much lower compared to graphite in sponge iron bath.

Besides dissolution data in sponge iron, Fig. 7 also contains the same for both the samples in electrolytic iron bath under identical experimental condition. This has been done to compare the kinetics of particular types of carbon when the bath composition is changed from pure (electrolytic iron) to commercial (sponge iron). It is very apparent from Fig. 7 that for both the samples, electrolytic iron offers less resistance compared to sponge iron bath towards dissolution. It is difficult to ascertain the exact reason for this retarding effect of sponge iron.

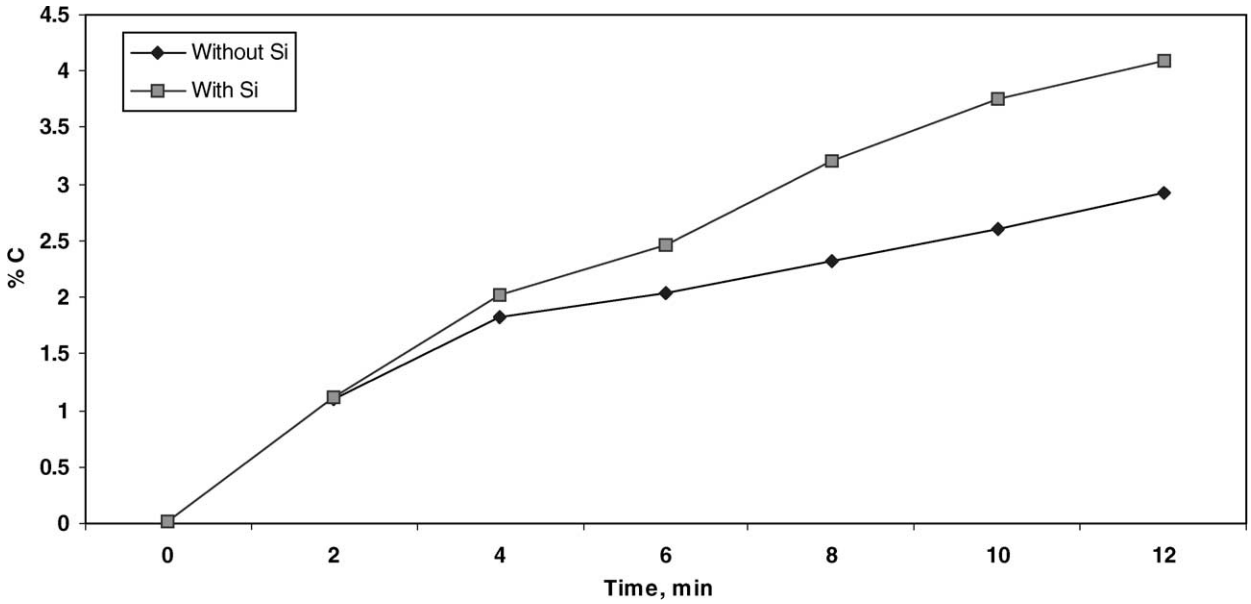

Fig. 5. Effect of silicon on dissolution of graphite in electrolytic iron bath.

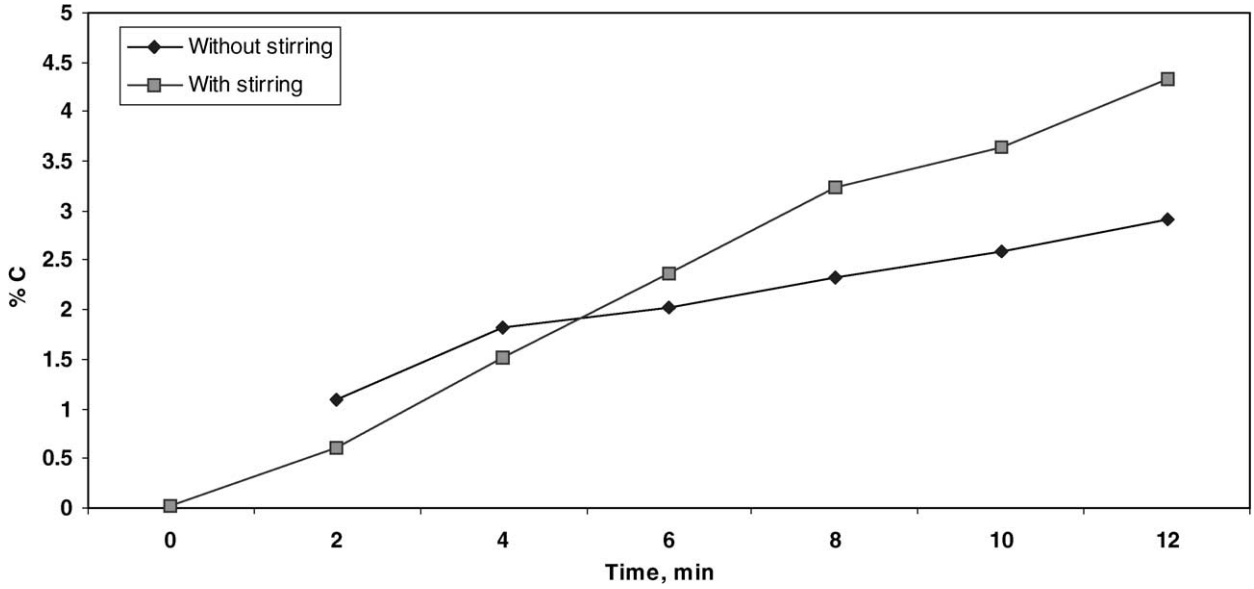

Fig. 6. Effect of stirring on dissolution of graphite in electrolytic iron bath.

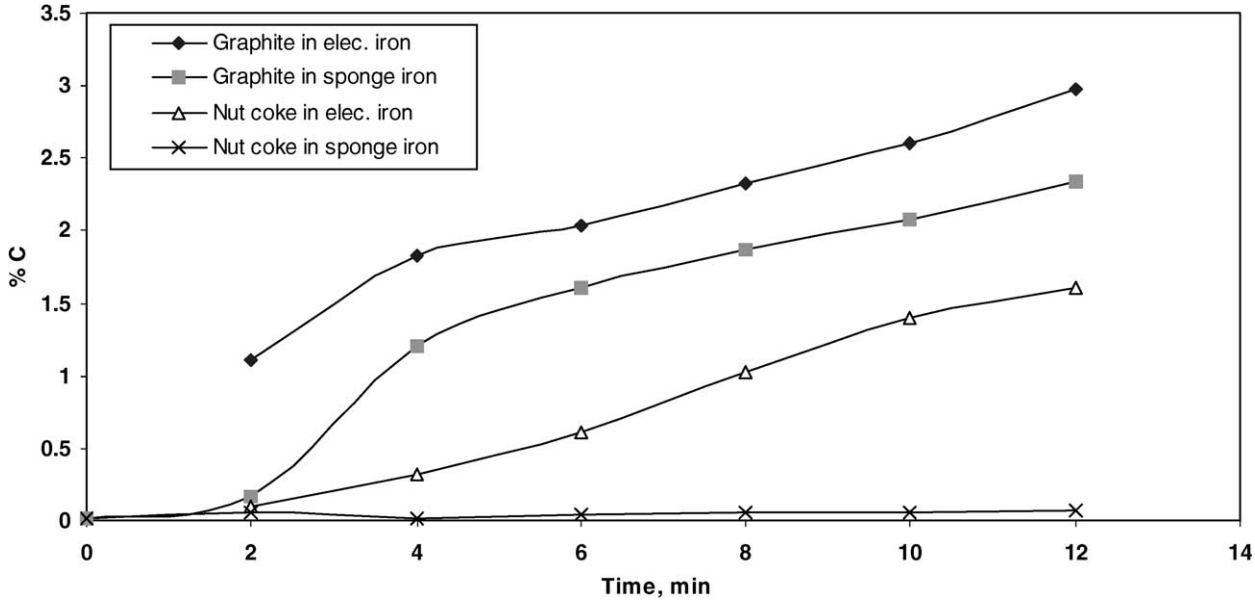

Fig. 7. Dissolution of graphite and nut coke in electrolytic and sponge iron bath at 1600 °C.

Nut coke dissolution rate appears to be severely affected by sponge iron. The impurities present in it is expected to exert interactive influence on transfer of carbon from solid to liquid bath. For example, Al_2O_3 is known to retard dissolution whereas SiO_2 promotes it. Further, a part of carbon which is dissolved in the bath will be consumed to reduce a portion of the impurity oxides from the iron bearing material and thus will not report in the bath. This will lead to lowering of bath carbon concentration. Again, sponge iron contains around 0.02% S and is further augmented by sulphur from nut coke resulting the final bath concentration to increase to around 0.04% which will depress dissolution. This further supports the negative influence of sulphur on carbon dissolution. The exact reason why graphite experiences less hindrace to dissolution in sponge iron bath could not be readily identified. However, less amount of ash and sulphur content in it may be responsible for this observation.

4. Mathematical analysis

Dissolution of carbonaceous material in liquid iron bath is primarily associated with three major phenomena (a) dissolution of solid carbon, (b) transfer of carbon from the

immediate vicinity of carbon surface to the bulk, and (c) transfer of heat from surrounding to the reaction site. Besides inherent kinetic parameters, the latter two items strongly influence the overall kinetics of the process and in turn, depend on the agitation condition of the bath. Even though the bath in Tamman furnace is termed as 'static bath', in true sense, this is not valid. Initially, the bath has uniform carbon, but as the dissolution progresses a concentration gradient will set up. Further, dissolution being endothermic in nature, temperature drop will take place around the sample. This will also result in establishing a temperature gradient at least near the carbon surface. These two factors together will generate natural convection in the bath and a recirculatory motion will be developed. In case of induction furnace, a strong circulation can be observed due to the presence of electromagnetic force. Characterisation of the bath in induction furnace demands very involved mathematical analysis and hence has not been attempted in the present exercise. Therefore, the following analysis is restricted to experiments in Tamman furnace only under conditions of natural convection.

In general, the rate of change of bath composition in terms of carbon can be expressed as

$$\frac{\mathrm{d}[\mathrm{C}]}{\mathrm{d}t} = \frac{kA_\mathrm{s}}{V_\mathrm{m}}\{[\mathrm{C}]_\mathrm{s} - [\mathrm{C}]_\mathrm{b}\} \quad (1)$$

where k is the mass transfer coefficient (cm/s), A_s the solid–liquid interfacial area (cm^2), V_m the volume of the melt (cm^3), $[\mathrm{C}]_\mathrm{s}$ the equilibrium or saturation carbon content of the bath, and $[\mathrm{C}]_\mathrm{b}$ is the carbon content in the bath at any time t.

Saturation carbon content of the bath as a function of temperature can be calculated from the following empirical correlation proposed by Chipman et al. [14]:

$$[\mathrm{C}]_\mathrm{s} = 1.34 + (2.54 \times 10^{-3})T \quad (2)$$

where T is in °C. In the case of sulphur bearing melts [15–17], a modified correlation is given as follows:

$$[\mathrm{C}]_\mathrm{s} = 1.34 + (2.54 \times 10^{-3})(T - 273) - 0.4[\%\mathrm{S}] \quad (3)$$

Integration of Eq. (1) yields,

$$-\ln\left\{\frac{[\mathrm{C}]_\mathrm{s} - [\mathrm{C}]_\mathrm{b}}{[\mathrm{C}]_\mathrm{s} - [\mathrm{C}]_0}\right\} = Kt \quad (4)$$

where $[\mathrm{C}]_0$ is the initial carbon concentration of bath, K (s^{-1}) the apparent mass transfer coefficient defined as

$$K = \frac{kA_\mathrm{s}}{V_\mathrm{m}} = \frac{k\rho A_\mathrm{s}}{W_\mathrm{m}} \quad (5)$$

If the rate equation is valid, then a plot of $-\ln\{([\mathrm{C}]_\mathrm{s} - [\mathrm{C}]_\mathrm{b}) / ([\mathrm{C}]_\mathrm{s} - [C]_0)\}$ versus t should yield straight lines and the slope of these plots will give apparent mass transfer coefficient K. With a knowledge of iron bath density, weight and also interfacial area, it is possible to calculate the mass transfer coefficient from correlation (5). Integrated rate plots under different experimental conditions were made as a function of time and few such plots are presented in Fig. 8. It may be noted that all the sample plots in the figure exhibit reasonable straight line relation indicating the validity of the rate equation. Similar plots in other experimental conditions follow identical trend.

The apparent rate constant K, calculated by regression analysis of the dissolution data are presented in Table 3. The table also contains the mass transfer coefficient (k) calculated from the correlation (5). Besides the overall mass transfer coefficient, k was also calculated as a function of cumulative time step. Time dependence of k for the same set of experiments as presented in Fig. 8 are illustrated in Fig. 9. The interfacial area in Eq. (5) was estimated based on the contact area between the sample and the melt. However, as the dissolution progresses, the diameter of the samples

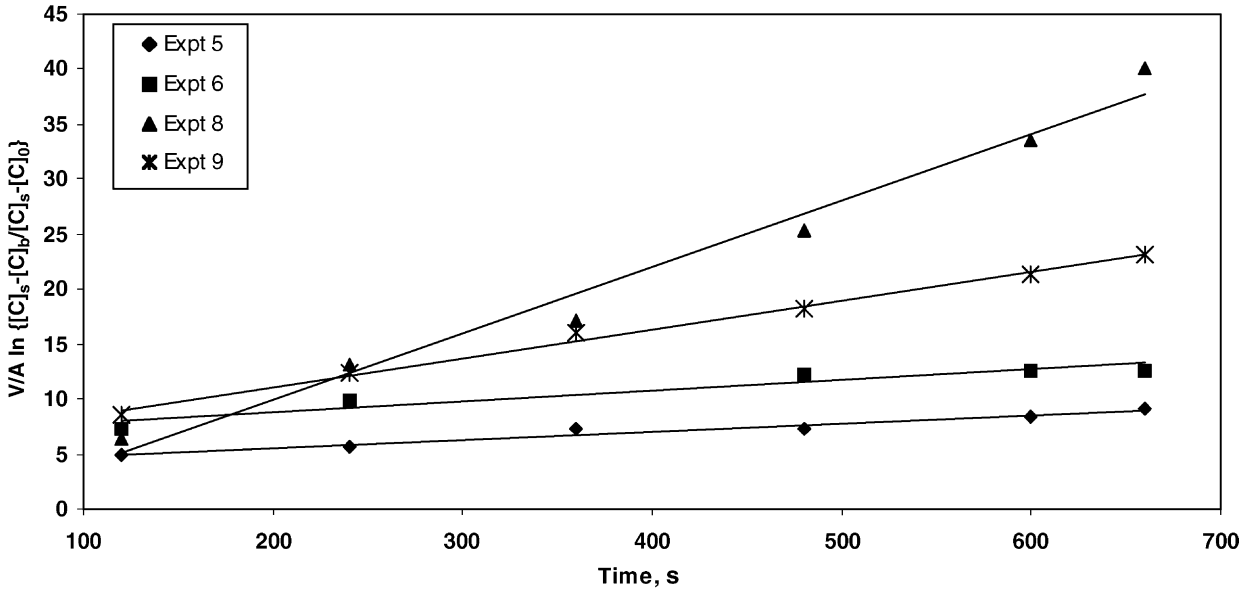

Fig. 8. Sample plots on V/A $\{([\mathrm{C}]_\mathrm{s} - [\mathrm{C}]_\mathrm{b}) / ([\mathrm{C}]_\mathrm{s} - [C]_0)\}$ against time under different experimental conditions.

Table 3
Apparent rate constant (K) and mass transfer coefficient (k) under different experimental conditions

Experiment number	T (°C)	Source of carbon	Type of bath	Remarks	K ($\times 10^{-3}$; s^{-1})	k ($\times 10^{-3}$; cm/s)
1	1550	Graphite	EI	–	−0.96	4.5
2	1600	Graphite	EI	–	−1.1	4.96
3	1650	Graphite	EI	–	−1.21	5.63
4	1600	Nut coke	EI	–	−0.53	2.4
5	1600	Coal	EI	–	−0.38	1.7
6	1600	Charcoal	EI	–	−0.53	2.5
7	1600	Graphite	EI	0.94% Si addition	−1.96	9.17
8	1600	Graphite	EI	0.05% S addition	−1.06	4.95
9	1600	Graphite	SI	–	−0.83	3.85
10	1600	Nut coke	SI	–	−0.001	0.005
11	1600	Graphite	EI	Stirring of bath	−2.2	10.36
12	1600	Pet coke	EI	–	−1.8	10.81
13	1600	Graphite	EI	0.42% Si, 0.02% S, 0.15% P addition	−1.69	7.88

EI: electrolytic iron; SI: sponge iron.

continuously reduces and so also the surface area. Dynamic monitoring of the change in diameter was a difficult task. Hence, the initial surface area values were assigned for the calculation of mass transfer coefficients.

It may be noted from Table 3 that for graphite, the value of k marginally increases with the increase in temperature. However, the k values for graphite in the present study appear to be almost half of the values reported by Kosaka and Minowa [5]. For example, Kosaka and Minowa have found the value of k to be 8.1×10^{-3} cm/s at 1548 °C in a SiC furnace in comparison to 4.5×10^{-3} cm/s for the present investigation. This apparent discrepancy is possibly because of the difference in the bath circulatory condition arising in the two types of heating units. In this connection, it is worth mentioning that even a mild rotation of the graphite rod at 35 rpm has been found to increase the mass transfer rate from 4.9×10^{-3} to 1.03×10^{-2} cm/s at 1600 °C.

The effect of sulphur on the dissolution of graphite in electrolytic iron at 1600 °C is not very clearly reflected in the k values. This is possibly because of the low amount of sulphur added to the bath (0.05%). But the marginally higher amount of sulphur in conjunction with the impurities present in the sponge iron decreases the k value from 4.9×10^{-3} to 3.8×10^{-3} cm/s.

On the contrary, Si is found to be a strong promoter of dissolution kinetics. When 0.94% Si is added to in the electrolytic iron bath, the value of k at 1600 °C is almost doubled. Even addition of 0.42% Si alongwith inhibitors (0.02% S and 0.15% P) increased the value of k by around 1.5 times over the value when no addition is made.

The apparent activation energy for the dissolution process was calculated by plotting $\ln k$ against the reciprocal of temperature in an Arrhenius plot and the value was found to be 10 kcal/mol. Orsten and Oeters [12] reported that the acti-

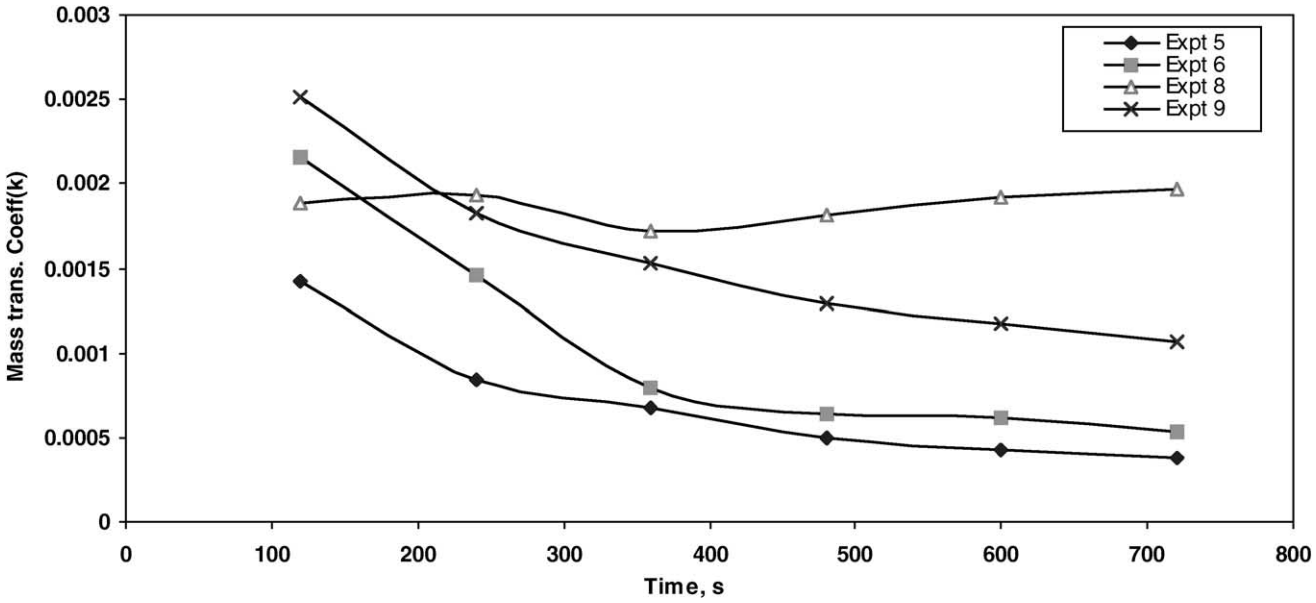

Fig. 9. Variation of mass transfer coefficient (k) against time for several experiments.

vation energy for dissolution of rotating electrode graphite cylinder in iron melt to be 18.6 kcal/mol. They concluded that mass transfer through liquid boundary layer controls the dissolution process. In the present scheme, the experiments were conducted by dipping the graphite samples in a static bath. The effect of boundary layer mass transfer on the dissolution kinetics is thus expected to be more prominent. Low activation energy in the present study indicates that boundary layer mass transfer is the rate controlling step for dissolution of graphite in static bath condition.

Further, with rotating graphite cylinder, the same investigators found that the phase boundary reaction rate is an order of magnitude higher than the mass transfer coefficient. Hence in the present experimental configuration, the phase boundary reaction appears not to impart any significant influence on the overall rate.

4.1. Heat transfer calculation

Dissolution of carbon in liquid iron bath is an endothermic reaction and the heat of solution ΔH can be given by the following equation [18]:

$$\mathrm{C(gr)} \rightarrow \mathrm{C(sat)}$$

$$\Delta H = 5400 + 5810(1 - X_{\mathrm{Fe}}^2) \tag{6}$$

where X_{Fe} is mole fraction of iron in the bath. In the case of Fe–C bath containing around 3% C, the heat of solution is expected to be around 6140 cal/mol and this will cause a temperature drop in the bath in course of dissolution. It is further assumed that the heat flux from the furnace is entirely consumed as the heat of dissolution of carbon in the boundary layer at the interface of the sample. The steady-state heat flux Q (cal/cm^2 s) under no heat loss condition is given as [5]

$$Q = \frac{\Delta H}{12}\frac{\mathrm{d}W}{\mathrm{d}t} = \frac{\Delta H}{12}\rho_{\mathrm{s}} V_{\mathrm{r}} = h\,\Delta T \tag{7}$$

where $\Delta T = T_{\mathrm{b}} - T_{\mathrm{s}}$ (°C) is the temperature drop across the boundary layer, T_{b} the bulk temperature (°C), T_{s} the interface temperature (°C), h the heat transfer coefficient (cal/°C s), V_{r} the rate of change of the radius of carbon (cm/s).

Many researchers have measured the periodic weight loss [5,11,12] or the change in carbon sample diameter [5] to supplement the bath carbon analysis in kinetic calculation. In the present study, weight change and the change in diameter as a function of time was monitored only for few experiments and are not used for our calculation. The reasons for not employing the earlier data may be described as follows.

(a) Periodic weight loss measurements of partially dissolved carbon sample involves withdrawal of the sample from melt and subsequent cooling in inert atmosphere. Our data analysis for preliminary experiments show that around 10–12% oxidation loss of sample occurred even when dissolution experiments were carried out with continuous dipping under inert atmosphere conditions. Withdrawal of hot carbon sample is expected to aggravate oxidation loss and hence rendering the integrity of the weight loss data doubtful.
(b) As reported in [11], intermittent dipping may affect the dissolution kinetics.
(c) Carbon was found to be dissolved nonuniformly giving rise to considerable difference in diameter longitudinally. For example, a 19.3-mm diameter graphite rod after 4 min of dissolution exhibits typical diameter range of 10–13 mm depending upon the location of measurement.

As a result of the earlier description, it was decided to estimate the rate of weight change as well as the rate of change in diameter through mathematical formulation in the following manner.

From a basic material balance of the bath,

$$\frac{\mathrm{d}G}{\mathrm{d}t} = \rho V_{\mathrm{m}}\frac{\mathrm{d[C]}}{\mathrm{d}t} = \rho k A_{\mathrm{s}}\{[\mathrm{C}]_{\mathrm{s}} - [\mathrm{C}]_{\mathrm{b}}\} \tag{8}$$

where $\mathrm{d}G/\mathrm{d}t$ is the rate of change of mass. Utilising Eq. (4),

$$[\mathrm{C}]_{\mathrm{s}} - [\mathrm{C}]_{\mathrm{b}} = \{[\mathrm{C}]_{\mathrm{s}} - [\mathrm{C}]_0\}\exp\left[\frac{-kA_{\mathrm{s}}t}{V_{\mathrm{m}}}\right]$$

Hence,

$$\frac{\mathrm{d}G}{\mathrm{d}t} = \rho k A_{\mathrm{s}}\{[\mathrm{C}]_{\mathrm{s}} - [\mathrm{C}]_0\}\exp\left[-\frac{kA_{\mathrm{s}}t}{V_{\mathrm{m}}}\right] \tag{9}$$

On integration, we obtain

$$\Delta G = G - G_0 = \rho V_{\mathrm{m}}\{[\mathrm{C}]_{\mathrm{s}} - [\mathrm{C}]_0\}(1 - \mathrm{e}^{-\alpha t}) \tag{10}$$

where ΔG is the change in weight of carbon in time t, G the weight of sample at time $t = t$, G_0 the initial weight of sample, and α equals $kA_{\mathrm{s}}/V_{\mathrm{m}}$.

The average rate of change in radius of the sample can be computed by the following Eq. (5):

$$V_{\mathrm{r}} = \left[1 - \frac{G_0 - \Delta G}{G_0}\right]\frac{d_0}{2t} \tag{11}$$

where d_0 is the initial diameter of the sample. Combining Eqs. (10), (11) and (7), we obtain the value of Q, the heat flux across the boundary layer. With a knowledge of heat transfer coefficient, h, in liquid iron bath, the unknown temperature drop due to dissolution of carbon can be calculated as

$$\Delta T = \frac{Q}{h} \tag{12}$$

The effect of endothermic heat of dissolution on the temperature drop across the thermal boundary layer at the interface between the carbon rod and the bath and hydrodynamics of the bulk melt have been analysed by making a thermal balance equating the heat flux from the furnace wall to the dissolution enthalpy following Eq. (7). The bath in the annular space between the carbon rod and the crucible is a vertical, cylindrical cavity whose vertical surfaces are

heated and cooled while the horizontal surfaces are insulated or adiabatic. The interface of the carbon rod with the bath acts as a heat sink and the outer surface of the crucible acts as a heat source with a uniform heat flux from the surface.

Extensive studies have been made by various researchers on determining the thermal and flow characteristics of the bath for these conditions. For uniform wall temperature, a thermal gradient is set up between the cooled surface and the heated surface, while for uniform heat flux at the wall, the gradient is set up within the boundary layer adjacent to the walls. Due to this thermal gradient, thermal buoyancy forces come into play and may set up convection currents.

The intensity of convection is dependent on the relative strength of the buoyancy and viscous forces which in turn depend on several factors such as the heat flux, the temperature drop, the thermal properties of the bath, etc. A convenient way to analyse the thermal state and convection of the bath is to construct a scale-invariant analysis by estimating several dimensionless numbers, namely, the Nusselt (*Nu*), Prandtl (*Pr*) and Grashof (*Gr*) number for bath conditions. Table 4 provides the definitions and interpretation of the earlier three dimensionless groups. *Gr* is the most important number indicating the level of free convection. Alternatively, a product of *Gr* and *Pr*, also called the Rayleigh number (*Ra*) is frequently used to quantify the effect of free convection on *Nu*. For small *Ra* ($Ra \leq 10^3$), the buoyancy driven flow is weak and conduction is the primary mode of heat transfer, signifying from Fourier's law, $Nu \approx 1$. For $Ra > 10^3$, the buoyancy forces are sufficiently stronger than the viscous forces and convection currents are set up in the cavity. A recirculatory or cellular flow characterises the buoyancy induced convection in which fluid ascends along the hot wall and descends along the cold wall and a thin boundary layer develops near the walls. The core of the fluid, however, remains nearly stagnant.

Table 4
Definition and interpretation of dimensionless groups for heat transfer and mass transfer

Dimensionless group	Definition	Interpretation
Nu	hL/λ	Dimensionless temperature gradient at the surface
Pr	$c\mu/\lambda$	Ratio of momentum and thermal diffusivities
Gr	$g\beta\,\Delta T\,L^3/\nu^2$	Ratio of buoyancy to viscous forces
Sh	kL/D_e	Dimensionless concentration gradient at the surface
Sc	$\mu/\rho D_e$	Ratio of momentum and mass diffusivity
Le	α/D_e	Ratio of thermal and mass diffusivity

A number of empirical correlations between *Nu*, *Pr*, and *Gr* have been reported in the literature for a variety of cavity geometries (such as a rectangular cavity, an annulus between concentric cylinders, etc.), the geometry of the hot and cold surfaces, the agitation condition of the bath and/or the surfaces such as rotating or static, etc. Table 5 provides a partial list of a few such correlations which have been especially used by past workers to analyse thermal conditions for dissolution of carbon in iron bath.

Although correlation (2) in Table 5 has been used for static bath by Kosaka and Minowa [5], it is not clear whether the earlier equation is applicable for convective heat transfer around a static cylinder. A preliminary calculation of *Nu* for the static cylindrical carbon rod and bath in Tamman furnace using the earlier equation yielded an overestimated

Table 5
A partial list of heat transfer correlations available in literature

Serial number	Correlation	Developed/used by	Remarks
1	$Nu = 0.125(Re)^{0.64}$	Izumi [19]	Used for carbon dissolution in rotating bath $10^3 < Re < 10^5$
2	(a) $Nu = 0.555(Gr \times Pr)(1/4)$ valid for$10^4 < Gr \times Pr < 10^8$ or (b) $Nu = 0.129(Gr \times Pr)(1/3)$ valid for $10^8 < Gr \times Pr < 10^9$	Kosaka and Minowa [5]	Used for carbon dissolution in static bath
3	$Nu = (Pr^{2/5}/(3.91 + 9.32Pr^{1/2} + 9.95Pr^{1/5}))Gr^{1/5}$	White [20]	Developed for uniform wall temperature and laminar flow in the boundary layer around a static cylinder
4	$Nu = 0.825 + 0.387(Gr \times Pr)^{1/6}/[1 + (0.492/Pr)^{9/16}]^{8/27}$, valid for $(D/L) \geq (35/Gr^{1/4})$ and for $10^{-1} < Ra < 10^{12}$	Churchill and Chu [21]	Developed for both laminar and turbulent regimes of flow under uniform wall temperature.
5	$(Nu^{1/2} - 0.85)Nu^{1/6} = 0.387(Gr \times Pr)^{1/6}/[1 + (0.492/Pr)^{9/16}]^{8/27}$	Ditto	Developed for the condition of uniform wall heat flux and around a vertical cylinder in an infinite fluid medium
6	(a) $Nu = 0.42(Ra)^{1/4}Pr^{0.012}(L/\bar{D})^{-0.3}$, valid for $10 < (L/D) < 40$, $1 < Pr < 2 \times 10^4$ and $10^4 < Ra < 10^7$ (b) $Nu = 0.046(Ra)^{1/3}$, valid for $1 < (L/D) < 40$, $1 < Pr < 20$ and $10^6 < Ra < 10^9$	Raithby and Holland [22]	Developed for free convection heat transfer in the annular space between long horizontal concentric cylinders.

Nu. Therefore, we sought a more appropriate correlation for *Nu* against *Ra* in the heat transfer literature.

The correlations listed in Table 5 are applicable for horizontal plates or cylinders. However, the crucible containing the iron bath inside a Tamann furnace is kept in a vertical position and experiences a uniform heat flux at the wall surfaces. For a vertical plate under uniform heat flux, no knowledge of temperature drop across the boundary layer is available a-priori. As a consequence, estimation of *Gr* is not possible according to its definition given in Table 5. Therefore, a modified *Gr* (Gr^*) is defined as [23]

$$Gr^* = Gr \times Nu = \frac{g\beta\,\Delta T\,L^3}{\nu^2}\frac{Q_w L}{\Delta T} = \frac{g\beta Q_w L^4}{k\nu^2} \tag{13}$$

where Q_{ws} is the wall heat flux. The *Ra* is likewise modified as

$$Ra = \frac{Gr^* \times Pr}{Nu} \tag{14}$$

With these definitions, correlation (5) in Table 5 is obtained by modifying correlation (4) in the same table, for the uniform wall heat flux conditions. In the earlier correlations developed for uniform wall heat flux, all the physical properties are evaluated at the film temperature $[T_s + T_b]/2$. However, our preliminary calculations showed that the temperature drop ΔT is usually $<1\,^\circ$C and hence little error is expected if properties are evaluated at the bulk temperature T_b.

The earlier analysis for uniform wall temperature and heat flux respectively is valid for following cases.

1. A thermal boundary layer which is much smaller than the cylinder radius.
2. Natural convection heat transfer around a vertical cylinder in an infinite fluid medium.

Whereas the first condition is satisfied for our present case, the second condition is strictly not valid as the carbon rod is confined within a cylindrical crucible. The convection is therefore set up within the annulus between the two concentric cylinders. Raithby and Holland [22] have considered free convection heat transfer in the annular space between long, horizontal concentric cylinders. A typical correlation developed by them for certain range of aspect ratio is given in Table 5. Several important observations have been made as follows.

(a) Flow in the annular region is characterised by two cells that are symmetric about the vertical midplane.
(b) The o.d. and i.d. of the annulus D_o and D_i, the effective annulus diameter $\bar{D} = (D_o - D_i)/2$ and the aspect ratio $L/\bar{D}$ play important roles. Correlation (6a and b) in Table 5 are valid for aspect ratio between 1 and 40. For larger aspect ratios, other similar correlations have been proposed [22].

However, before the earlier correlations are applied, a correction for the *Ra* needs to be made on the basis of the effective dimensional factor of the annulus based on the i.d. and o.d. as follows:

$$Ra_c = \frac{[\ln(D_o/D_i)]^4}{\bar{D}^3(D_i^{-3/5} + D_o^{-3/5})^5} Ra \tag{15}$$

The equation is valid for the range $10^2 \le Ra_c \le 10^7$.

Likewise the effective thermal conductivity λ_{eff} is defined as the thermal conductivity that a stationary fluid should have to transfer the same amount of heat as the moving fluid. The suggested correlation for the effective thermal conductivity is given as follows [24]:

$$\frac{\lambda_{eff}}{\lambda} = 0.386\left(\frac{Pr}{0.861 + Pr}\right)^{1/4}(Ra_c)^{1/4} \tag{16}$$

4.2. Mass transfer calculation

As a consequence of the diffusive and convective flux of carbon from the interface of the carbon sample to the bulk, a mass density gradient would exist in the fluid. This would result in spatial variation of the fluid composition and the fluid density. A solutal buoyancy current may be set up in the fluid which in the case of the carbon sample would oppose the thermal buoyancy. A coupled analysis of the thermo-solutal or double diffusive convection is complex involving solution of Navier–Stokes and energy balance equations and is beyond the scope of the present analysis.

A convenient way to judge the strength of the solutal buoyancy is to evaluate a *Gr* defined as

$$Gr_m = \frac{L^3 g\,\Delta\rho\,\rho_s^2}{\mu^2} \tag{17}$$

where the buoyancy factor ($\Delta\rho$), defined as follows, decides the strength of the solutal buoyancy

$$\Delta\rho = \frac{\rho - \rho_s}{\rho} \tag{18}$$

forces in comparison with the viscous forces. In the equation, ρ_s is the density of carbon saturated iron melt (g/cm^3).

Our prelimiary calculation reveals that the buoyancy factor varies between 0.02 and 0.05 indicating a weak solutal buoyancy field. Under this condition, transfer of carbon may be assumed to have negligible influence on the free convection flow. Heat transfer correlations such as those described in the earlier sections could be used to determine the heat transfer coefficient. If additionally, Lewis number (*Le*), defined as the ratio of the Schmidt number (*Sc*) and the *Pr*, is approximately 1, the analogy between the heat and mass transport can be directly utilised. This implies that the set of equations involving dimensionless numbers which holds good for heat transfer is analogous to the correlations describing the mass transfer process with a different set of dimensionless numbers. More specifically, the *Nu* will be replaced by Sherwood number (*Sh*), the *Pr* by the *Sc* and the *Gr* by its equivalent as defined in Table 4 and Eq. (17).

However, for larger values of Le ($Le \gg 1$), the direct analogy of heat and mass transfer does not hold. For this case, the mass transfer coefficient is obtained from the heat transfer coefficient as follows

$$\frac{h}{k} = \frac{\lambda}{D_e L_e^{1/3}} \quad (19)$$

In order to utilise Eq. (19) for calculation of mass transfer coefficient, a few parameters namely λ, D_e, μ and $\Delta\rho$ need to be evaluated a-priori. The density of the iron melt (ρ) can be evaluated using the following expression available in [12]:

$$\rho = 8.750 - 6.96 \times 10^{-4}[\mathrm{C}] - 1.15 \times 10^{-3}(T - 273) \quad (20)$$

The viscosity μ of liquid Fe–C alloy depends on the bath carbon content and also on the temperature of the bath. The value of viscosity of the liquid in near vicinity of the carbon surface where the melt will be carbon saturated is of interest for the present study. This can be obtained by extrapolating data available for low carbon melt [5] to the level of carbon saturation and is given by [11]:

$$\mu = 10^{[-4.31+(4874/T)]} \quad (21)$$

The value of carbon diffusion coefficient D_e in carbon saturated iron bath is not available. However, the same can be calculated using the following general expression [11]:

$$D_e = 2.5 \times 10^{-14}\frac{T}{\mu} \quad (22)$$

The value of the specific heat of liquid iron is taken from the monograph of Ida and Guthrie [25]. In absence of any data on thermal conductivity of liquid Fe–C bath, the value reported for liquid steel [25] has been used for our calculation.

5. Results of mathematical analysis

The characteristics of natural convection heat transfer around the carbon rod inside the cylindrical crucible is analogous to the free convection heat transfer in an annulus between two concentric vertical cylinders under uniform wall heat flux from the Tamman furnace to the crucible. In order to verify whether the condition of uniform wall heat flux holds, Q was evaluated as follows. Firstly, the weight loss of the carbon rod was computed using Eq. (10) and the corresponding rate of change of rod diameter was evaluated using Eq. (11). Next, the endothermic heat of dissolution was obtained using Eq. (6). Finally, heat flux Q was computed using Eq. (7). A plot of Q against time is shown in Fig. 10. It is apparent that Q has negligible change with time. Therefore, the condition of uniform wall heat flux holds good for analysis of Tamman furnace data.

In order to obtain the dimensionless numbers, Nu, Pr and Ra which depend on the thermal conductivity λ, the effective thermal conductivity was evaluated for the annulus between concentric cylinders (that is, the carbon rod and the crucible) from the expression given in (23). Subsequently, Pr and Ra were evaluated based on the Gr^* as defined by correlation (3) in Table 5. The Ra was subsequently corrected taking into account the effective dimensional factor of the annulus following Eq. (15) for Ra_c. After ascertaining the magnitude of the Ra_c, Pr and $L/\bar{D}$, the Nu was then computed from the appropriate correlation (6a) in Table 5. The convective heat transfer coefficient h was obtained from the Nu. At this stage, it was necessary to ascertain whether mass transfer coefficient would be evaluated based on a direct analogy with the heat transfer correlation or from the Eq. (19).

In order to make a prudent judgement, the buoyancy factor, defined as per Eq. (18), was evaluated to ascertain the

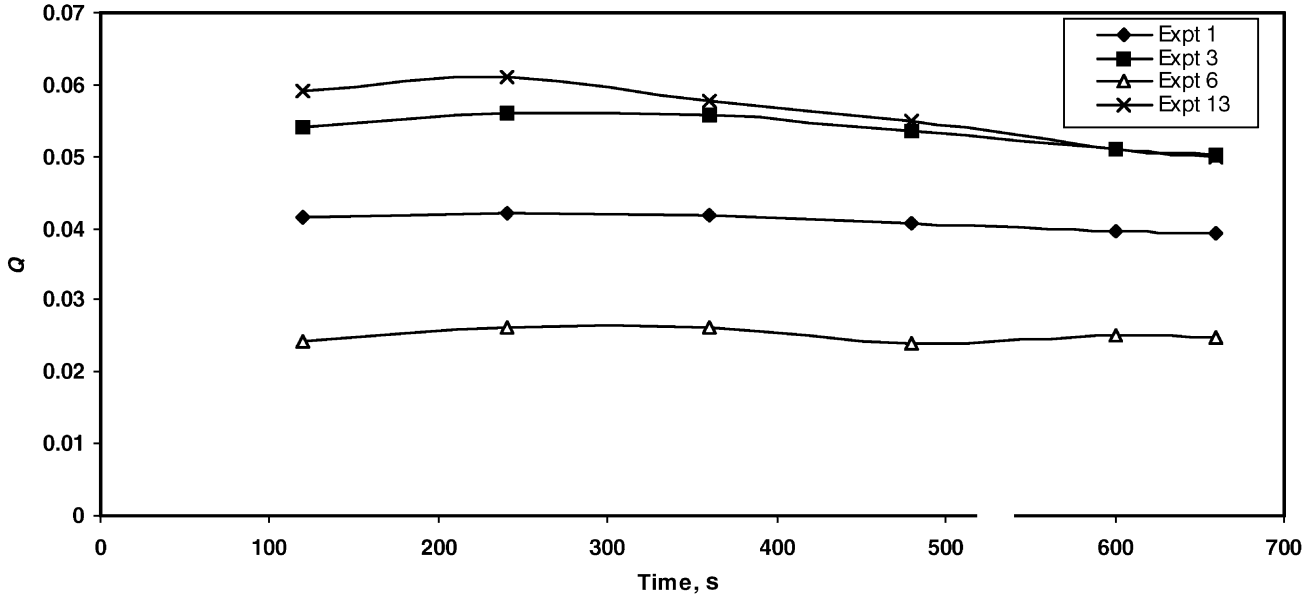

Fig. 10. Sample plots on variation of heat flux (Q) against time.

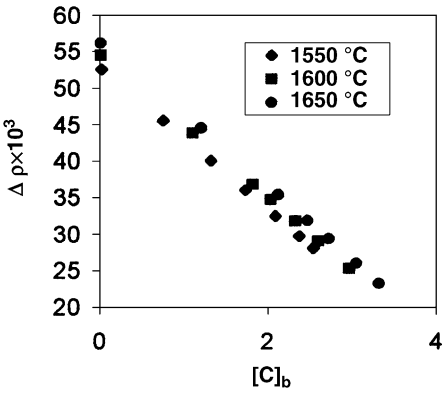

Fig. 11. Buoyancy factor vs. carbon concentration.

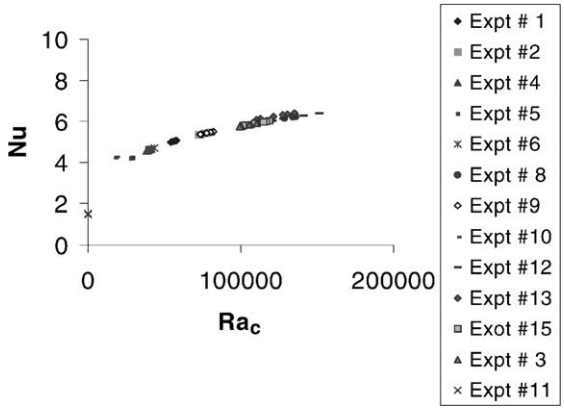

Fig. 12. A plot of *Nu* vs. modified *Ra* for various experimental runs.

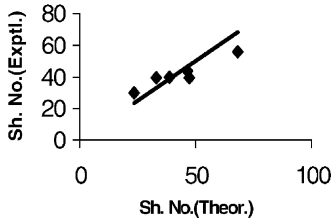

Fig. 13. A plot of experimental *Sh* vs. theoretical *Sh*.

strength of solutal buoyancy forces vis-à-vis the thermal convection and viscous forces. It was found that $\Delta\rho$ values for our data set was <0.05. Fig. 11 depicts the variation of $\Delta\rho$ against bath carbon concentration. It clearly shows that as the carbon concentration in the bath increases progressively with time towards the saturation concentration value, the strength of the buoyancy forces weakens. Moreover, there is a weak dependence of the solutal buoyancy factor on the temperature. Although, the weak dependence of solutal buoyancy on thermal buoyancy would merit use of an analogy between the heat and mass transfer correlations, it was necessary to check the magnitude of the *Le* such that it remains close to 1. On checking the *Le*, it was found that the order of magnitude of *Le* for our dataset was $>10^2$. Therefore, the direct analogy between the dimensionless correlations for the heat and mass transfer were shunned. Instead, the mass transfer coefficient was obtained from Eq. (19).

From the experimental data, the apparent mass transfer coefficient, *K* was obtained by plotting $-\ln\{[C]_s - [C]_b/([C]_s - [C]_0)\}$ against time. From the straight line plot, *K* was obtained by linear regression and yielded the mass transfer coefficient as per Eq. (5). The theoretical mass transfer coefficients were initially calculated on the basis of Eq. (19) upon evaluating the heat transfer coefficient on the basis of Eq. (6a) in Table 5. It was found that the theoretical *k* estimated as earlier was grossly underestimated in comparison with the experimental *k* values especially beyond $Ra_c \approx 10^4$. In view of the earlier, we undertook a rigorous non-linear regression study and obtained a correlation for *k* in terms of dimensionless numbers as follows.

(a) The effect of the bath chemistry in terms of percentage sulphur, phosphorus and silicon was incorporated in the form a parameter *C*.
(b) The *Nu* is expressed in terms the modified Ra_c, *Pr*, aspect ratio $(L/\bar{D})$ and the bath chemistry factor *C* as follows:

$$Nu = CRa_c^{1/4} Pr^{0.012} \left(\frac{L}{\bar{D}}\right)^{-0.3} \quad (23)$$

(c) On combining the earlier correlation and Eq. (19), the following dimensionless correlation for *Sh* results:

$$Sh = CRa_c^{1/4} \mathrm{Pr}^{0.12} \left(\frac{L}{\bar{D}}\right)^{-0.3} Le^{1/3},$$
$$\text{where } C = 0.15(\%S) + 0.18(\%P) + 0.018(\%Si) + 0.023 \quad (24)$$

Fig. 12 depicts the *Nu* calculated using Eq. (23) against modified *Ra* for various experiments conducted. Fig. 13 compares the experimental values of mass transfer coefficient against the theoretical values calculated using Eq. (24) in the form of dimensionless *Sh*. The fit obtained on regression was very high as evident from the R^2 value of 0.91. Although the correlation is similar to that of Raithby and Holland [22], the introduction of a modified Ra_c which takes into account the annular cylindrical geometry and the bath chemistry factor *C* have clearly contributed to an improvement in prediction of mass transfer of carbon in the iron bath.

6. Conclusions

In the present investigation, it has been found that the ash content in the carbonaceous materials has very significant influence on the dissolution kinetics. Contrary to the literature reporting, no noteworthy effect of the volatile matter on the dissolution process could be noticed in the present study. Increase in temperature helps to promote the dissolution rate.

Surface active agent like silicon has been observed to promote the rate of dissolution. However, the depressing effect of sulphur on rate could not be established possibly due to the low addition. Preliminary results of a mathematical model indicates that the dissolution process is mass transfer controlled and in the present experimental condition, takes place under constant heat flux condition. A correlation has been developed for the first time between dimensionless *Sh*, modified *Ra*, *Pr* and *Le*, which accounts not only for the geometry of the bath and the sample, but also the chemistry of the bath and gives a fairly accurate prediction of the mass transfer in the bath.

Acknowledgements

The research group wishes to acknowledge the active support of Prof. P. Ramachandra Rao, Director, NML, Jamshedpur and Prof. A.K. Mohanty, Principal REC, Rourkela in course of this study. Financial support from Extramural Research Fund, Council of Scientific and Industrial Research, India is gratefully acknowledged.

References

[1] R.V. Viley, Foundry Trade J. 20 (1951) 331.
[2] J. Ckikel, H. Miketta, Freiberger Forscungsh, Series B 3 (1953) 56.
[3] R. Krzeszewski, Gie Berei 46 (1959) 417.
[4] R.G. Olsson, V. Koump, T.F. Parzak, Trans. AIME 236 (1966) 426.
[5] M. Kosaka, S. Minowa, Trans. ISIJ 8 (1968) 392.
[6] S. Orsten, F. Oeters, Proc. Process Technol. Conf. (1988) 31.
[7] Ch. Hisatsuna, T. Shinodd, Sh. Sae, Imonology 37 (4) (1965) 27.
[8] C.F. Loper, S.L. Liu, S. Shirvani, T.W. Witter, Trans. AFS 92 (1984) 323.
[9] N. Kayama, O. Ishikawa, Imonology 37 (4) (1965) 278.
[10] J.K. Wright, B.R. Baldock, Met. Trans. 19 B (1988) 375.
[11] M.B. Mourao, G.G. Krishnamurthy, J.F. Elliot, Met. Trans. 24 B (1993) 629.
[12] S. Orsten, F. Oeters, in: Proceedings of the 5th International Iron and Steel Congress Process Technology, Book 3, Washington, DC, 1986, p. 143.
[13] L. Kalvelage, J. Markert, J. Poetschke, Arch. Eisenhuttnwes 50 (1979) 107.
[14] J. Chipman, R.A. Alfred, L.W. Gott, R.B. Small, D.M. Wilson, C.N. Thomson, D.L. Guernsky, J.C. Fulton, Trans. ASM 44 (1952) 1215.
[15] E.T. Turkdogan, R.A. Hancock, J. Iron Steel Inst. 179 (1955) 155.
[16] M. Ohtani, N.A. Gokcen, Trans. Met. Soc, AIME 218 (1960) 380.
[17] P.O. Mellberg, Li. Yunzu, Scand. J. Met. 10 (1981) 92.
[18] J.F. Elliot, M. Geiser, V. Ramakrishna, Thermochemistry for Steelmaking, Addison-Wesley, London, 1963, p. 500.
[19] K. Izumi, Nippon Kikaigakkai Ronbunsyn 17 (1955) 95.
[20] F.M. White, Fundamentals of Heat Transfer, Addison-Wesley, New York, 1988.
[21] S.W. Churchill, H.H.S. Chu, Int. J. Heat Mass Trans. 18 (1975) 1323.
[22] G.D. Raithby, K.G.T. Holland, Advances in Heat Transfer, Vol. 11, Academic Press, 1975, p. 265.
[23] M.N. Ozisik, Heat Transfer—A Basic Approach, McGraw Hill, New York, 1985.
[24] F.P. Incropera, D.P. Dewit, Fundamentals of Heat and Mass Transfer, Addison-Wesley, New York, 1998.
[25] T. Ida, R.I.L. Guthrie, The Physical Properties of Liquid Metals, Oxford University Press, Oxford, 1988.